ACS APPLIED MATERIALS & INTERFACES

Research Article

www.acsami.org

Resistive Switching and Modulation of $Pb(Zr_{0.4}Ti_{0.6})O_3$/Nb:$SrTiO_3$ Heterostructures

Yu Bai,[†,‡] Zhan Jie Wang,[*,†,‡,§] Yan Na Chen,[†] and Jian Zhong Cui[§]

[†]Shenyang National Laboratory for Materials Science, Institute of Metal Research, Chinese Academy of Sciences, Shenyang 110016, China

[‡]School of Materials Science and Engineering and [§]Key Laboratory of Electromagnetic Processing of Materials (Ministry of Education), Northeastern University, Shenyang 110819, China

Supporting Information

ABSTRACT: In this work, epitaxial $Pb(Zr_{0.4}Ti_{0.6})O_3$ (PZT) thin films with different thicknesses were deposited on Nb-doped $SrTiO_3$ (NSTO) single-crystal substrates by chemical solution deposition (CSD), and their ferroelectric resistive switching behaviors were investigated. The results showed that the maximum ON/OFF ratio up to 850 could be obtained in the PZT/NSTO heterostructure with the 150 nm thick PZT film. On the basis of the Schottky-Simmons model and the modified semiconductor theory, we also evaluated the interfacial built-in field and the depletion layer at the PZT/NSTO interface, which can be modulated strongly by the ferroelectric polarization, but are independent of the thickness of the PZT thin films. It is clear that the ferroelectric resistive switching is related to the ferroelectric polarization and modulated by the thickness of ferroelectric films. Therefore, there is an optimal thickness of the PZT film for the maximum ON/OFF ratio due to the ferroelectricity and conductivity mutually restricting. It can be expected that by adjusting the ferroelectricity and conductivity of the ferroelectric thin film and its thickness, the maximum switching ratio can be further improved.

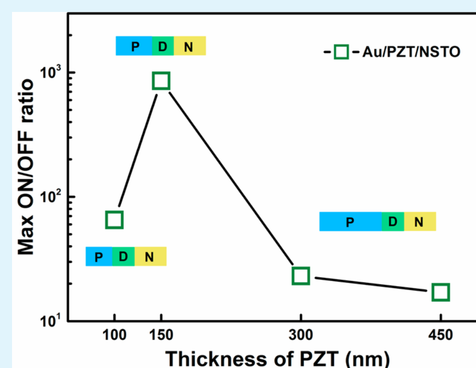

KEYWORDS: *ferroelectric heterostructures, resistive switching behaviors, ON/OFF ratio, ferroelectric polarization, interfacial built-in field*

1. INTRODUCTION

The resistive switching modulated by ferroelectric polarization is called ferroelectric resistive switching (RS),[1,2] which is intriguing for the potential application in next-generation nonvolatile memories.[1] The ferroelectric RS effect has been revealed in many ferroelectric thin films[3−5] and ferroelectric tunneling junctions (FTJs) based on ferroelectric ultrathin films.[6−10] Although the FTJs have been reproducibly demonstrated to present a remarkable resistive switching effect, the thickness requirement of the ferroelectric layer to be several nanometers greatly limits the potential applications.[1] In addition, for typical ferroelectric ultrathin films, large lattice mismatch, size effect, and structural defects could damage the ferroelectricity and cause a large leakage current, which could make the switching signal unreadable.[7,11] On the other hand, excellent electric properties such as high ON/OFF ratio, good retention, and high endurance have been reported in relatively thick ferroelectric thin films, such as $BiFeO_3$ (BFO),[12,13] $Pb(Zr_xTi_{1-x})O_3$ (PZT),[14,15] and $BaTiO_3$ (BTO).[4,16] For instance, Tsurumaki et al.[12] fabricated Pt/BFO (100 nm)/$SrRuO_3$ (SRO) layered structures on $SrTiO_3$ (STO) single-crystal substrates, and showed a ON/OFF ratio of above 1000. Hu et al.[13] reported a continuously tunable ON/OFF ratio up to 5000 in Pt/BFO (60 nm)/Nb-doped STO (NSTO) structure, which was attributed to the ferroelectric polarization modulation of the width of depletion layer at the BFO/NSTO interface. They suggested that the thin dielectric layer formed between Pt and BFO layer played a crucial role in the emergence of the resistive switching effect. Hou et al.[15] found that the ON/OFF ratio of 30 nm thick PZT films could be high as 10^6, which was achieved by a controllable filamentary behavior. Zhang et al.[16] obtained a ON/OFF ratio of 300 nm thick BTO films above 3 orders of magnitude, and observed an apparent variation in Schottky barriers in response to polarization switching, indicating a ferroelectric-related resistive switching effect.

The correlation between the ferroelectric RS behavior and ferroelectric polarization in the relatively thick ferroelectric films is different from that of the FTJs, and a variety of different microscopic mechanisms have been proposed to explain the resistive switching effect, such as the conductive filament type and the interface type modulated by ferroelectric polarization. However, the performance and mechanisms vary greatly, even for the same material and device structure.[5,12,14,15] For these

Received: September 1, 2016
Accepted: November 15, 2016
Published: November 15, 2016

 © 2016 American Chemical Society

DOI: 10.1021/acsami.6b10992
ACS Appl. Mater. Interfaces 2016, 8, 32948−32955

ferroelectric semiconducting films, the ferroelectricity and conductivity are directly determined by the thickness of ferroelectric films. To enhance the device performance, it is a main approach to modulate the potential barrier height or barrier thickness by ferroelectric polarization at the ferroelectric/electrode interfaces, which is also closely related to the thickness of ferroelectric films. Therefore, the thickness of ferroelectric films is a key factor in the regulation of the competition between the ferroelectric and conductive properties of the ferroelectric film. In addition, more direct experimental results are needed to demonstrate that the resistive switching behavior is based on the modulation effect of ferroelectric polarization.[13,17,18] Therefore, to achieve a large value of ferroelectric resistive switching in the relatively thick ferroelectric thin films, and further clarify the correlation between the ferroelectric RS and ferroelectric polarization, it is necessary to make clear the influence of the thickness of ferroelectric films.

In this study, we prepare $Pb(Zr_{0.4}Ti_{0.6})O_3/Nb:SrTiO_3$ (PZT/NSTO) heterostructures by chemical solution deposition, and investigate their resistive switching behaviors. The interfacial built-in field and the depletion layer at the PZT/NSTO interface are also evaluated by the Schottky-Simmons model and the modified semiconductor theory. The magnitude of the interfacial built-in field and the width of the depletion layer at the PZT/NSTO interface region can be modulated strongly by the ferroelectric polarization, but are independent of the thickness of the PZT thin films. The resistive switching is modulated by the ferroelectric polarization, and the maximum ON/OFF ratio up to 850 can be obtained in the PZT/NSTO heterostructure with the 150 nm thick PZT film. Therefore, the thickness of PZT film is a critical factor in modulating the resistive switching behavior of PZT/NSTO heterostructures due to the ferroelectricity and conductivity being mutually restricting. Our results show that modulation of the thickness of ferroelectric thin films is an effective way to improve the resistance switching performance of this kind of ferroelectric resistance switch devices.

2. EXPERIMENTAL DETAILS

Nb-doped $SrTiO_3$ single-crystal substrates ($Nb:SrTiO_3$ with 0.7 wt % of Nb, abbreviated as NSTO) were prebaking at 600 °C for 20 min to obtain a clear and stabilized surface. Epitaxial $Pb(Zr_{0.4}Ti_{0.6})O_3$ (PZT) thin films with thicknesses of 100, 150, 300, and 450 nm were grown on the NSTO substrates by chemical solution deposition (CSD). The details of the CSD process has been described clearly in our previous papers.[19,20] High-purity titanium tetra-isopropoxide ($Ti((CH_3)_2CHO)_4$), lead acetate ($Pb(CH_3COO)_2$), zirconium-*n*-propoxide ($Zr(OCH_2CH_2CH_3)_4$), and 2-propanol ($(CH_3)_2CHOH$) were used to prepare the precursor solution. The final concentration of the solution was adjusted to 0.4 M with the atomic ratio of Pb:Zr:Ti = 1.1:0.4:0.6. After aging for 24 h, the solution was spin-coated onto the NSTO substrates, operated at 4000 rpm for 30 s. The coated films were dried at 120 °C for 10 min and then pyrolyzed at 350 °C for 10 min. To obtain the PZT thin films with different thicknesses, the above steps were repeated several times before annealing. Finally, the perovskite PZT films were obtained by annealing in an electric furnace at 600 °C for 30 min. Top electrodes of Au with a diameter of 0.5 mm were deposited by sputtering on the surface of the PZT film to form a metal/ferroelectric/semiconductor sandwich structure.

The crystal structure and orientation of the PZT/NSTO heterostructures were analyzed by $\theta-2\theta$ scans of X-ray diffraction (XRD; Rigaku RINT2000, Cu $K\alpha$ radiation). The chemical composition of the PZT thin films was analyzed by X-ray photoelectron spectroscopy (XPS; Therma ESCALAB 250; Al $K\alpha$ source, energy step 0.1 eV). The microstructures of PZT films were characterized by transmission electron microscopy (TEM; Tecnai G2 F20). The TEM specimens were prepared by the standard procedure of cutting, gluing, slicing, grinding, and finally ion milling with Ar ions until they were electron-transparent by using a Gatan precision ion-polishing system (PIPS 691; Gatan). The ferroelectric properties and current−voltage characteristics of the films were measured by using a standard ferroelectric testing system (TF2000E; Aixacct). The built-in electric field and the depletion layer at the PZT/NSTO interface region were analyzed by the Schottky-Simmons model and the modified semiconductor theory.

3. RESULTS AND DISCUSSION

The chemical composition of the PZT thin films was analyzed by X-ray photoelectron spectroscopy, and is in accord with the expected stoichiometric ratio (Figure S1, Supporting Information). The crystal structure and orientation of the PZT films with different thicknesses on the NSTO substrate were studied by XRD. Figure 1 shows the XRD pattern of the PZT film with

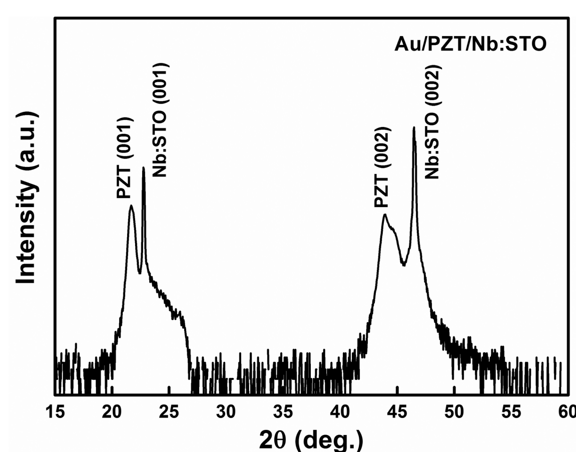

Figure 1. XRD pattern of the PZT film with 150 nm thickness on the NSTO substrate.

the thickness of 150 nm. Only strong and sharp diffraction peaks of the (00*l*) plane for the perovskite phase can be detected in the PZT film, implying that the PZT films have grown epitaxially on the (00l)-orientated NSTO substrate. The effect of strain status on the PZT/NSTO heterostructures was also investigated. The calculated lattice mismatch between PZT and NSTO is about 3.2% based on the standard lattice constants of PZT (a_{PZT} = 0.404 nm) and NSTO (a_{NSTO} = 0.391 nm). Thus, the PZT films on the NSTO substrate are under compressive stress in the in-plane direction. Moreover, the strain status does not depend on the thickness of PZT films because there is no peak shift in the XRD patterns of the PZT films with different thicknesses (Figure S2). This result can be explained by the critical thickness for strain relaxing. Stemmer et al. have reported that the critical thickness of PZT films for the misfit dislocation formation is about 50 nm.[21] Thus, the PZT films with thickness ranging from 100 to 450 nm are expected to be fully relaxed. To further characterize the epitaxial nature of the PZT/NSTO heterostructures, the TEM study has also been conducted. Figure 2a shows a cross-sectional TEM image of the PZT/NSTO heterostructure with the 150 nm thick PZT layer. The interface between the PZT layer and the NSTO substrate is clear and there are no intermediate layers or phase. Figure 2b shows a high-resolution TEM (HRTEM) image of the PZT/NSTO interface. It can be

DOI: 10.1021/acsami.6b10992
ACS Appl. Mater. Interfaces 2016, 8, 32948−32955

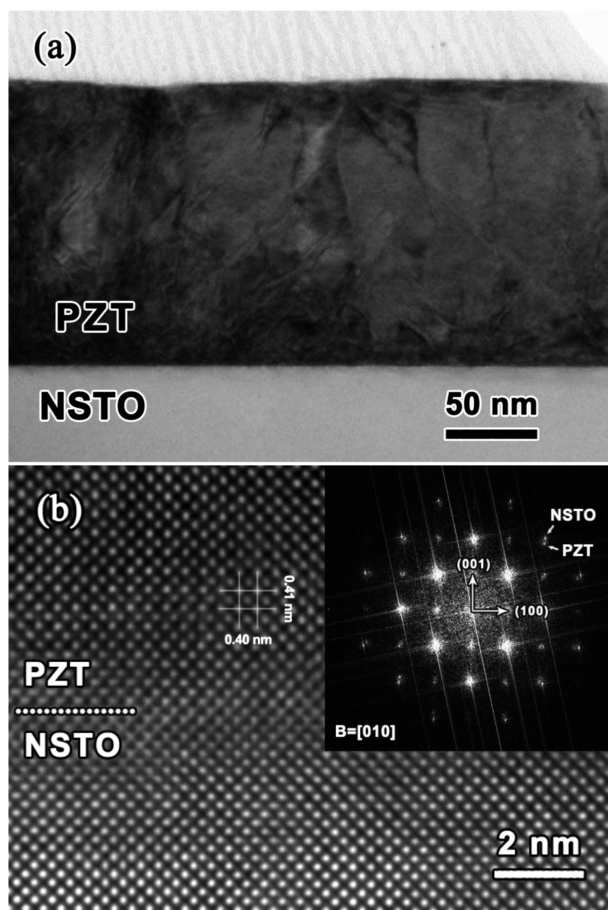

Figure 2. (a) Cross-sectional TEM image for the PZT film with 150 nm thickness. (b) High-resolution TEM image of the PZT/NSTO interface. The inset shows the fast Fourier transform (FFT) patterns transformed from the HRTEM image.

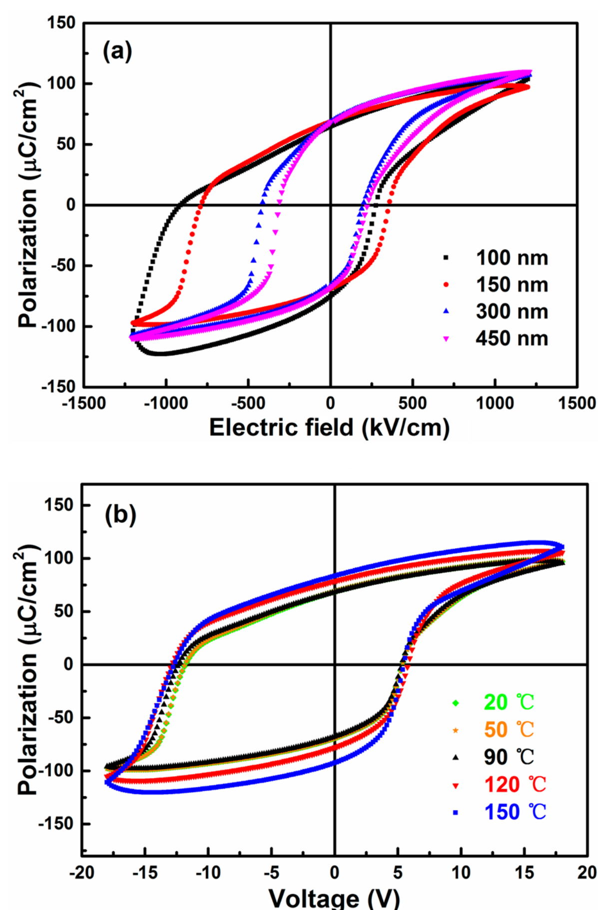

Figure 3. (a) P–E characteristics of the Au/PZT/NSTO heterostructures with the different thicknesses of PZT film at a frequency of 100 Hz. (b) P–V characteristics of the Au/PZT(150 nm)/NSTO heterostructure measured at different temperatures at a frequency of 100 Hz.

seen that the high-quality PZT film has grown epitaxially on the top of NSTO. The fast Fourier transform (FFT) patterns (the inset in Figure 2b) show that the orientation relationship between the PZT layer and the NSTO substrate is $(001)_{PZT}//(001)_{NSTO}$ and $(100)_{PZT}//(100)_{NSTO}$. In addition, the c and a values for the perovskite PZT phase are determined to be 0.41 and 0.40 nm, respectively, which are consistent with those of the bulk PZT. The above XRD and TEM results demonstrate that high-quality PZT/NSTO heterostructure films are obtained to discuss the intrinsic interfacial phenomena.

The polarization–electric field (P–E) characteristics of the PZT films were investigated, and the results are shown in Figure 3. Figure 3a shows the P–E hysteresis loops of PZT films with different thicknesses measured at room temperature. The remanent polarization for all the samples are almost the same, namely, is almost not depending on the film thickness. The large remanent polarization (about 70 μC/cm^2) also signifies that the crystal quality of the PZT thin films is very good. However, with decreasing the thickness, the P–E hysteresis loops distorted at the part of negative electric field, and the coercive fields significantly increased. Usually, the asymmetry of P–E hysteresis loop of ferroelectric films is caused by the use of different top and bottom electrode materials.[22] In this situation, the positive and negative coercive voltage would simultaneously increase with decreasing the thickness of ferroelectric films. However, in this study, the Au and NSTO electrodes are the same for all the samples, but only the negative coercive voltage increases with decreasing the PZT thickness, indicating the distorted P–E hysteresis loops and the increased coercive fields are mainly related to the interface-controlled electric field at the PZT/NSTO interface. Generally, an interfacial electric field can be induced by the oxygen vacancy in the ferroelectric films,[23] stress gradient at the ferroelectric/electrode interface,[24] and domain pining by a intrinsic electric field.[25] If we consider the influence of defect dipoles in the interfacial defective layer, the shape of the P–E hysteresis loop may change unpredictably.[26,27] It has also been demonstrated that the defect dipoles can respond to the external electric field at high temperatures (>120 °C) and switch with the polarization switching.[28] However, in this study, the shapes of polarization–voltage hysteresis loops remain unchanged with increasing the measured temperature up to 150 °C, despite the polarization value slightly increasing due to the increase in leakage current caused by bits of thermal charge injection (Figure 3b). In addition, as mentioned above, the XRD and TEM results (Figures 1 and 2) show that the PZT film has grown epitaxially on the NSTO substrate, and there is no interfacial defective layer in the interface region of PZT/NSTO. On the other hand, although all the PZT films are in the same stress status, the shift of hysteresis loops strongly depends on the thickness of PZT films. Therefore, the stress gradient is also not a major influential factor to cause the

DOI: 10.1021/acsami.6b10992
ACS Appl. Mater. Interfaces 2016, 8, 32948–32955

coercive voltage asymmetry. As a result, it can be concluded that the interfacial electric field at the PZT/NSTO heterostructure is an intrinsic built-in electric field which could cause domain pinning, leading to the asymmetric hysteresis loops.

To investigate the resistive switching behavior in the PZT/NSTO heterostructure, typical current−voltage ($I-V$) measurements were carried out by sweeping the applied voltage as shown in Figure 4a. The resistive switching behavior is observed in the PZT/NSTO heterostructure with the 150 nm thick PZT film. To ensure the repeatability of the resistive switching behavior, the bias was swept continuously several times and the results are almost the same. The process of resistive switching from a low-resistance state (LRS) to a high-resistance state (HRS) begins at about +6.5 V, which corresponds to the coercive voltage of about +6.0 V in Figure 3b. In contrast, the process of the resistance switching from the HRS to the LRS is at about −13.0 V, which corresponds to the coercive voltage of about −12.5 V in Figure 3b. In addition, the $I-V$ curve also exhibits an asymmetric feature which is similar to the $P-V$ hysteresis loops (Figure 3b), proving that the resistive switching behavior is related to the ferroelectric polarization. In addition to the bipolar resistive switching, the samples also show rectifying behavior, especially for the voltage within −5 to 5 V.

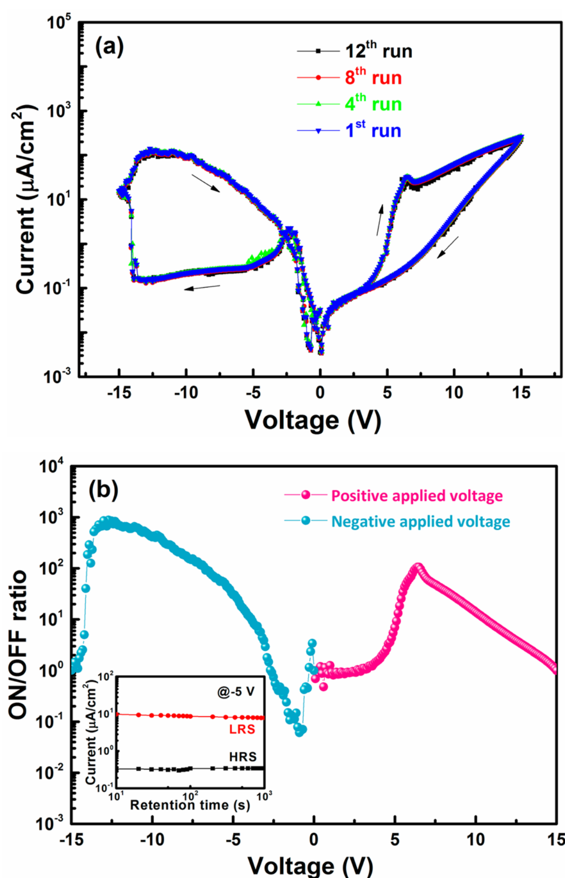

Figure 4. (a) $I-V$ curves for the Au/PZT(150 nm)/NSTO heterostructure. (b) The ON/OFF ratio as a function of reading voltage which is extracted from the $I-V$ data of Figure 4a. The inset shows the retention characteristics.

Figure 4b shows the ON/OFF ratios of the PZT/NSTO heterostructure. It can be seen that the maximum ON/OFF ratio is 106 for the positive voltage at +6.4 V and is 856 for the negative voltage at −13.5 V. Namely, the resistive switching effect can be tuned up to about 10^3, which is compared with previous reports.[6,29,30] However, most of these results were achieved in the PZT/NSTO heterostructure obtained by pulse laser deposition (PLD), which is difficult for deposition of uniform large-area films for practical applications. Until now, such high ON/OFF ratio is rarely reported in the PZT/NSTO heterostructure obtained by chemical solution deposition. Moreover, it should be noted that electroformation is not required before the observation of $I-V$ hysteresis loops. Also, the retention test was carried out at −5 V after application of two opposite applied bias to set the LRS or HRS, as shown in the inset of Figure 4b. The ON/OFF ratio remained stable for about 10^3 s with a minor reduction, which provides additional evidence that the resistive switching in the PZT/NSTO films is a nonvolatile effect.

Several mechanisms have been suggested to explain the resistive switching behaviors in ferroelectric films.[5,12,31,32] As mentioned above, we have excluded the defect-mediated mechanisms (ionic or electronic) for resistive switching in the PZT/NSTO heterostructures. Thus, the mechanism for the resistive switching in the PZT/NSTO heterostructures can be discussed by the built-in electric field at the PZT/NSTO interface using the Schottky-Simmons model and the modified semiconductor theory.[22] To map out the distribution of the built-in electric field in the PZT/NSTO heterostructure, we analyzed the current−voltage ($I-V$) characteristics in the full LRS (from −2 to 2 V) of the PZT/NSTO heterostructure according to the approach proposed by Pintilie et al.[33,34] and Das et al.[35] Figure 5a shows the leakage current as a function of the measured temperature. The leakage current in the negative voltage part increases with increasing the measured temperature from 50 to 190 °C, and is used to reveal the basic conductive mechanisms of the PZT/NSTO heterostructure. In ferroelectric films, according to dominant conduction routes for carriers, several conductive mechanisms have been proposed, such as Schottky emission, Frenkel-Poole emission, Fowler-Nordheim tunneling, and space charge limited current (SCLC).[36−38] In the PZT/NSTO heterostructure, according to the above analysis results, the possible carrier injection mechanism is dominated by the potential barrier at the PZT/NSTO interface. The possibility of Fowler-Nordheim tunneling as the current mechanism is basically ruled out due to the obvious temperature dependence of the $I-V$ characteristics. Therefore, the interface-controlled current is mainly due to the Schottky emission. Thus, the leakage current density can be obtained by the following equation:[39,40]

$$J = 2q\left(\frac{2\pi m_{\mathrm{eff}}KT}{h^2}\right)^{3/2}\mu E\,\exp\left(-\frac{q}{kT}\left(\varphi_{\mathrm{B}}^{0} - \sqrt{\frac{qE_{\mathrm{m}}}{4\pi\varepsilon_0\varepsilon_{\mathrm{op}}}}\right)\right) \quad (1)$$

where q is the electron charge, h is Planck's constant, m_{eff} is the effective mass, T is the temperature, k is the Boltzmann's constant, μ is the mobility of electrons in the conduction band of the PZT, E is the electric field in the bulk PZT, E_{m} is the maximum field at the interface if a Schottky-like contact is present (depletion region width is voltage-dependent), φ_{B}^{0} is the potential barrier at zero bias, ε_0 is the vacuum permittivity, and $\varepsilon_{\mathrm{op}}$ is the dielectric constant at optical frequencies of PZT which is ~6.5. According to eq 1, the plots of $\ln(J/T^{3/2})$ versus the reciprocal temperature ($1000/T$) for the different applied

DOI: 10.1021/acsami.6b10992
ACS Appl. Mater. Interfaces 2016, 8, 32948−32955

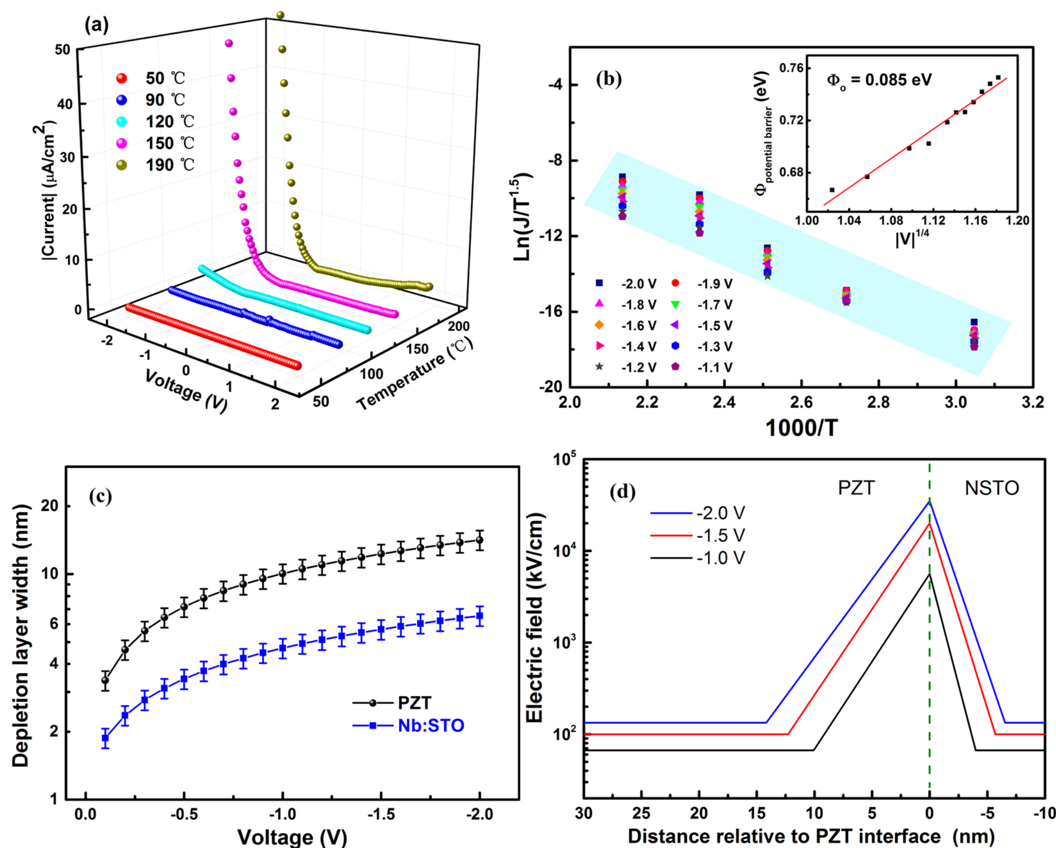

Figure 5. (a) *I*−*V* curves for the Au/PZT (150 nm)/NSTO heterostructure measured at different temperatures from 50 to 190 °C. (b) Schottky-Simmons representation of the negative applied voltage range for LRS. The inset indicates the zero applied voltage Schottky barrier heights at the PZT/NSTO interface. (c) Voltage dependence of the depletion layer widths for the Au/PZT(150 nm)/NSTO heterostructures. (d) Electric field distribution at the PZT/NSTO interface under different applied electric fields.

voltages are shown in Figure 5b, and the potential barrier at a relevant voltage can be estimated from the slop. In this way, we can obtain different potential barriers at different temperatures from 1.0 to 2.0 V every 0.1 V intervals. The relationship between E_m and V is given by the following equation:[39]

$$E_m = \sqrt{\frac{2qN_{eff}(V + V_{bi})}{\varepsilon_0 \varepsilon_{op}}} + \frac{P}{\varepsilon_0 \varepsilon_{st}} \tag{2}$$

Here, N_{eff} is the effective density of charge in the depleted region of the PZT thin film, V_{bi} is the built-in potential, P is the ferroelectric polarization, and ε_{st} is the relative dielectric constant of PZT which is ~500 in our samples. Compared with the available references,[33,40,41] the $P/\varepsilon_0\varepsilon_{st}$ term in eq 2 is negligible and then the potential barriers at several applied voltages can be plotted as a function of $V^{1/4}$, as shown in the inset in Figure 5b. Because of the good linear fit, the potential barrier at zero voltage can be estimated from the intercept to be 0.085 eV, which means that the potential barrier is so intensively modulated by polarization charges. According to the Schottky-Simmons equation and the fitting results, the magnitude of E_m is obtained by the following equation:

$$E_m = \frac{4\pi\varepsilon_0 \varepsilon_{op}(\Delta\varphi)^2}{q} \tag{3}$$

And the distribution of E_m is represented by the width of the depletion layer according to the basic formula of semiconductor heterostructure as shown in the following equations:[25,42]

$$V_{PZT\text{-}bi} = \frac{\varepsilon_{NSTO} N_D}{\varepsilon_{NSTO} N_D + \varepsilon_{PZT} N_{eff}} (V_{bi} + V) \tag{4-1}$$

$$V_{NSTO\text{-}bi} = \frac{\varepsilon_{NSTO} N_{eff}}{\varepsilon_{NSTO} N_D + \varepsilon_{PZT} N_{eff}} (V_{bi} + V) \tag{4-2}$$

$$W_{PZT} = \sqrt{\frac{2\varepsilon_{PZT}\varepsilon_{NSTO} N_D (V_{PZT\text{-}bi} + V)}{qN_{eff}(\varepsilon_{NSTO} N_D + \varepsilon_{PZT} N_{eff})}} \tag{4-3}$$

$$W_{NSTO} = \sqrt{\frac{2\varepsilon_{PZT}\varepsilon_{NSTO} N_{eff} (V_{NSTO\text{-}bi} + V)}{qN_D(\varepsilon_{NSTO} N_D + \varepsilon_{PZT} N_{eff})}} \tag{4-4}$$

Here, the electron concentration N_D is 2×10^{20} cm^{-3} in 0.7 wt % Nb-doped STO, and the effective dopant concentration N_{eff} of the PZT is 10^{20} cm^{-3}.[25] It is assumed that the relative dielectric constants of PZT and NSTO are constants (ε_{PZT} is ~500 and ε_{NSTO} is ~50 in our samples) under a relatively low applied voltage. Figure 5c shows the width of the depletion layer as a function of the applied voltage. The width of the depletion layer increases with the increase of the voltage, but the change law is a parabola characteristic. Hypothesizing that the electric field outside the depletion layer is approximately equal to the applied electric field, the distribution of the built-in electric field in the PZT/NSTO heterostructure can be described as shown in Figure 5d. It can be seen that the built-in electric field is 10−100 times the applied electric field and slightly increases as the positive bias applied to the NSTO. Moreover, a depletion layer formed at the PZT/NSTO

DOI: 10.1021/acsami.6b10992
ACS Appl. Mater. Interfaces 2016, 8, 32948−32955

interface with the built-in electric field, and the width of the depletion layer changes with the change of the internal electric field. The built-in electric field and the width of the depletion layer are no relation to the PZT thickness.

The built-in electric field in the PZT/NSTO heterostructure and its effects on the ferroelectric polarization and resistive switching behavior can be explained by the band structures of the PZT/NSTO heterostructures. Figure 6a is a schematic of the Au/PZT/NSTO capacitor and shows that the ferroelectric polarization in the PZT film is upward (P_{up}) after applying a positive electric field. If we consider the PZT and NSTO as wide band gap semiconductors and without considering the polarization charges, the band structure of the PZT/NSTO heterostructure can be described as in Figure 6b. For NSTO, the values of electron affinity and energy band gap are 4.0 and 3.2 eV, respectively. Because of the high conductivity of NSTO, its Fermi level is close to the bottom of the conduction band. Namely, NSTO should be an n-type semiconductor and its work function is 4.2 eV.[18,43] For PZT, the values of electron affinity and energy band gap are 3.5 and 3.4 eV, respectively. According to many research results, PZT should be a p-type semiconductor due to the Pb loss. Thus, its Fermi level is below, but close to the middle of the energy band gap, and its work function is 5.8 eV.[25,44] Owing to the difference in work functions, the energy band bends across the PZT/NSTO interface. Thus, an induced built-in electric field (E_{bi}) pointing from NSTO to PZT has formed across the interface, which is similar to a semiconductor p-n junction, and a depletion layer has formed in the PZT layer near the PZT/NSTO interface. However, PZT is not just a p-type semiconductor, but is also a ferroelectric. If we consider the ferroelectric polarization of the PZT thin film, the above situation will be changed. When the ferroelectric polarization in the PZT layer is downward (P_{down}) after applying a negative electric field, the positive polarization charges appear at the PZT/NSTO interface region. Thus, the majority carriers in the NSTO will be attracted to the PZT/NSTO interface region by the positive polarization charges, so the built-in electric field (E_{bi}) and the width of the depletion layer decrease, as shown in Figure 6c. This condition corresponds to the LRS in the resistive switching behavior (Figure 4a). In contrast, when the ferroelectric polarization is upward (P_{up}) after applying a positive electric field, the negative polarization charges aggregate at the PZT/NSTO interface region. Thus, the majority carriers in the NSTO are repelled by the negative polarization charges and migrate away from the interface region, so the built-in electric field (E_{bi}) and the width of depletion layer increase, as shown in Figure 6d. This condition corresponds to the HRS in the resistive switching behavior (Figure 4a). In addition, although the magnitude of the built-in electric field can be modulated strongly by the ferroelectric polarization, the direction of the built-in electric field remains unchanged.

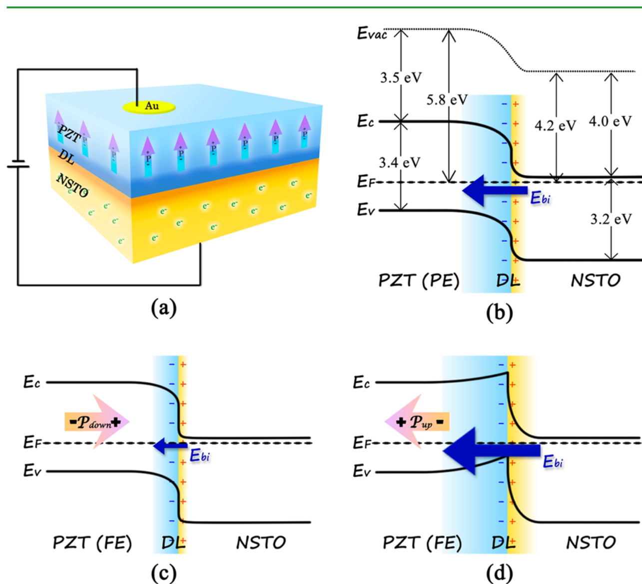

Figure 6. (a) Schematic of the Au/PZT/NSTO heterostructure under an applied electric field (DL represents "depletion layer"). (b−d) Band structure diagrams for the PZT/NSTO heterostructure in the different states: (b) in the state without considering the polarization, (c) in the state of polarization downward (LRS), and (d) in the state of polarization upward (HRS).

It has been a controversial issue that the resistive switching behavior is based on the modulation effect of ferroelectric polarization.[13,17,18] However, in this study, we have presented the direct relation between the voltage for the maximum ON/OFF ratio and the ferroelectric coercive voltage (Figure 4). Therefore, it can be considered that the modulation effect of ferroelectric polarization on the width of depletion layer (Figure 6c,d) induces the two states of the LRS and the HRS in the resistive switching behavior.

On the other hand, as mentioned above, there is an interfacial electric field at the PZT/NSTO interface like the p-n junction. The direction of the interfacial electric field is always from NSTO to PZT, leading to the hard switchable domains forming at the PZT layer near the PZT/NSTO interface. Therefore, the hysteresis loops would present asymmetry because the interfacial domains tend to P_{up} rather than P_{down} (Figure S3). However, the magnitude of the built-in electric field and the width of the depletion layer at the PZT/NSTO interface region are not related to the PZT thickness; namely, the proportion of the ferroelectric domains inside the depletion layer to those outside the depletion layer is impacted by the thickness of the PZT films. In a thicker PZT film, the width of depletion layer will take a smaller proportion relative to the thickness of the PZT film; thus, the effect of the ferroelectric domains inside the depletion layer on the total ferroelectric polarization switching will be weakened, which correspond to our results (Figure 3a) that the negative coercive voltage decreases with increasing the thickness of PZT film, while the positive coercive voltage does not change greatly. Therefore, the resistive switching behaviors for the PZT/NSTO heterostructures will be affected by the PZT thickness because the resistive switching is closely related to the polarization switching.

The initial $I-V$ curves for the PZT/NSTO heterostructures with different thicknesses were measured (Figure S4). Figure 7 shows the maximum ON/OFF ratio of the PZT/NSTO heterostructures as a function of the PZT thickness (P represents PZT, D represents the depletion layer, and N represents NSTO). The result indicates that the maximum ON/OFF ratio increases with decreasing the thickness of PZT film, and then decreases after reaching the peak at 150 nm. When the PZT film is too thin, the depletion layer occupies a considerable proportion in the PZT film so that the modulation effect of ferroelectric polarization on the depletion layer becomes smaller. Thus, the value of the ON/OFF ratio decreases in the thinner films. In contrast, although the

DOI: 10.1021/acsami.6b10992
ACS Appl. Mater. Interfaces 2016, 8, 32948−32955

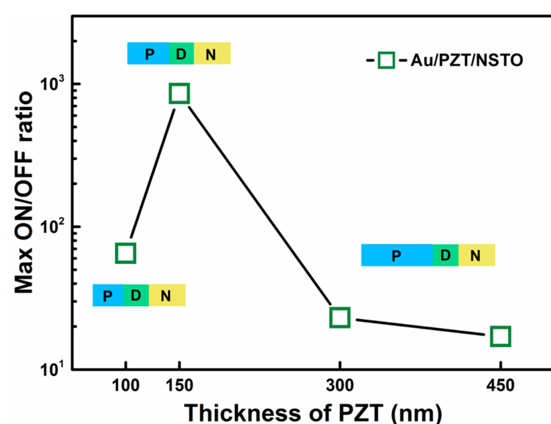

Figure 7. Maximum ON/OFF ratio of the PZT/NSTO heterostructure as a function of the PZT thickness (P represents PZT, D represents depletion layer, and N represents NSTO).

modulation effect of ferroelectric polarization on the depletion layer may become powerful in the thicker films, the conductive property of PZT films tends to decrease with increasing their thickness. In this situation, the volume resistance becomes crucial compared to the interfacial effect, which also decreases the ON/OFF ratio. Therefore, there is an optimal thickness of the PZT film for the largest ON/OFF ratio. As shown in Figure 7, the optimal thickness of the PZT layer for the largest ON/OFF ratio is around 150 nm. It is clear that the resistive switching behavior of the PZT/NSTO heterostructures depends on the competition of the ferroelectricity and conductivity of the PZT film, and can be modulated by controlling the thickness of the PZT film. Although the maximum switching ratio of the PZT/NSTO heterostructure is not too high in this study, we believe that it can be further improved greatly by adjusting the ferroelectricity and conductivity of the PZT thin film and its thickness. Our results demonstrate that the modulation of the thickness of ferroelectric thin films is an effective way to improve the resistance switching performance of this kind of ferroelectric resistance switch devices. Especially, for designing new material systems, the proper thickness of ferroelectric films should be thought first to balance the ferroelectricity and conductivity.

4. CONCLUSION

In this study, we achieved the ferroelectric resistive switching up to about 850 in the PZT/NSTO heterostructure, which was prepared by chemical solution deposition with the 150 nm thick PZT films. The correlations between $P-V$ and $I-V$ curves, coercive field, and voltage of maximum ON/OFF ratio clearly demonstrated the modulation effect of ferroelectric polarization on resistive switching. We also explored the interfacial built-in field in the PZT/NSTO heterostructures based on the Schottky-Simmons model and the modified semiconductor theory. The magnitude and distribution of the electric field across the PZT/NSTO heterostructure were evaluated. Combined with the band structures of the PZT/NSTO heterostructure, the variations of interfacial built-in electric field were clarified. The magnitude of the interfacial built-in field and the width of the depletion layer were modulated strongly by ferroelectric polarization, but the direction of the interfacial built-in field was unchanged in the PZT/NSTO heterostructure, which are all independent of the PZT thickness. The relative thickness that is strongly related to the ON/OFF ratio must be taken into consideration to modulate resistive switching behavior of ferroelectric−semiconductor heterostructures.

■ ASSOCIATED CONTENT

Supporting Information

The Supporting Information is available free of charge on the ACS Publications website at DOI: 10.1021/acsami.6b10992.

XPS spectra of the PZT films, XRD patterns of the PZT/NSTO heterostructures with different PZT layer thicknesses, schematic diagrams of domain pinning, and $I-V$ curves of the Au/PZT/NSTO films with different PZT thicknesses (PDF)

■ AUTHOR INFORMATION

Corresponding Author

*E-mail: wangzj@imr.ac.cn.

ORCID

Zhan Jie Wang: 0000-0002-9288-4928

Notes

The authors declare no competing financial interest.

■ ACKNOWLEDGMENTS

The partial support of this work by the Hundred Talents Program of Chinese Academy of Sciences, and the National Natural Science of Foundation of China (Nos. 51172238 and 51502303) is gratefully acknowledged.

■ REFERENCES

(1) Garcia, V.; Bibes, M. Ferroelectric Tunnel Junctions for Information Storage and Processing. *Nat. Commun.* **2014**, *5*, 4289.

(2) Zhuravlev, M. Y.; Sabirianov, R. F.; Jaswal, S. S.; Tsymbal, E. Y. Giant Electroresistance in Ferroelectric Tunnel Junctions. *Phys. Rev. Lett.* **2005**, *94*, 246802.

(3) Zhang, L.; Chen, J.; Cao, J.; He, D.; Xing, X. Large Resistive Switching and Switchable Photovoltaic Response in Ferroelectric Doped $BiFeO_3$-Based Thin Films by Chemical Solution Deposition. *J. Mater. Chem. C* **2015**, *3*, 4706−4712.

(4) Li, M.; Zhou, J.; Jing, X.; Zeng, M.; Wu, S.; Gao, J.; Zhang, Z.; Gao, X.; Lu, X.; Liu, J. M.; Alexe, M. Controlling Resistance Switching Polarities of Epitaxial $BaTiO_3$ films by Mediation of Ferroelectricity and Oxygen Vacancies. *Adv. Electron. Mater.* **2015**, *1*, 1500069.

(5) You, T.; Du, N.; Slesazeck, S.; Mikolajick, T.; Li, G.; Burger, D.; Skorupa, I.; Stocker, H.; Abendroth, B.; Beyer, A.; Volz, K.; Schmidt, O. G.; Schmidt, H. Bipolar Electric-Field Enhanced Trapping and Detrapping of Mobile Donors in $BiFeO_3$ Memristors. *ACS Appl. Mater. Interfaces* **2014**, *6*, 19758−19765.

(6) Radaelli, G.; Gutierrez, D.; Sanchez, F.; Bertacco, R.; Stengel, M.; Fontcuberta, J. Large Room-Temperature Electroresistance in Dual-Modulated Ferroelectric Tunnel Barriers. *Adv. Mater.* **2015**, *27*, 2602−2607.

(7) Wang, L.; Cho, M. R.; Shin, Y. J.; Kim, J. R.; Das, S.; Yoon, J. G.; Chung, J. S.; Noh, T. W. Overcoming the Fundamental Barrier Thickness Limits of Ferroelectric Tunnel Junctions through $BaTiO_3$/$SrTiO_3$ Composite Barriers. *Nano Lett.* **2016**, *16*, 3911−3918.

(8) Wen, Z.; Li, C.; Wu, D.; Li, A.; Ming, N. Ferroelectric-Field-Effect-Enhanced Electroresistance in Metal/Ferroelectric/Semiconductor Tunnel Junctions. *Nat. Mater.* **2013**, *12*, 617−621.

(9) Hu, W. J.; Wang, Z.; Yu, W.; Wu, T. Optically Controlled Electroresistance and Electrically Controlled Photovoltage in Ferroelectric Tunnel Junctions. *Nat. Commun.* **2016**, *7*, 10808.

(10) Bilc, D. I.; Novaes, F. D.; Iniguez, J.; Ordejon, P.; Ghosez, P. Electroresistance Effect in Ferroelectric Tunnel Junctions with Symmetric Electrodes. *ACS Nano* **2012**, *6*, 1473−1478.

(11) Jiang, L.; Choi, W. S.; Jeen, H.; Dong, S.; Kim, Y.; Han, M.-G.; Zhu, Y.; Kalinin, S. V.; Dagotto, E.; Egami, T.; Lee, H. N. Tunneling Electroresistance Induced by Interfacial Phase Transitions in Ultrathin Oxide Heterostructures. *Nano Lett.* **2013**, *13*, 5837−5843.

(12) Tsurumaki, A.; Yamada, H.; Sawa, A. Impact of Bi Deficiencies on Ferroelectric Resistive Switching Characteristics Observed at P-Type Schottky-Like Pt/$Bi_{1-\delta}FeO_3$ Interfaces. *Adv. Funct. Mater.* **2012**, *22*, 1040−1047.

(13) Hu, Z.; Li, Q.; Li, M.; Wang, Q.; Zhu, Y.; Liu, X.; Zhao, X.; Liu, Y.; Dong, S. Ferroelectric Memristor Based on Pt/$BiFeO_3$/Nb-Doped $SrTiO_3$ Heterostructure. *Appl. Phys. Lett.* **2013**, *102*, 102901.

(14) Liu, W. W.; Jia, C. H.; Zhang, Q.; Zhang, W. F. Mechanism of Rectification and Two-Type Bipolar Resistance Switching Behaviors of Pt/$Pb(Zr_{0.52}Ti_{0.48})O_3$/Nb:$SrTiO_3$. *J. Phys. D: Appl. Phys.* **2015**, *48*, 485102.

(15) Hou, P.; Wang, J.; Zhong, X.; Wu, Y. A Ferroelectric Memristor Based on the Migration of Oxygen Vacancies. *RSC Adv.* **2016**, *6*, 54113−54118.

(16) Zhang, F.; Lin, Y.-B.; Wu, H.; Miao, Q.; Gong, J.-J.; Chen, J.-P.; Wu, S.-J.; Zeng, M.; Gao, X.-S.; Liu, J.-M. Asymmetric Reversible Diode-Like Resistive Switching Behaviors in Ferroelectric $BaTiO_3$ thin Films. *Chin. Phys. B* **2014**, *23*, 027702.

(17) Wang, C.; Jin, K. J.; Xu, Z. T.; Wang, L.; Ge, C.; Lu, H. B.; Guo, H. Z.; He, M.; Yang, G. Z. Switchable Diode Effect and Ferroelectric Resistive Switching in Epitaxial $BiFeO_3$ Thin Films. *Appl. Phys. Lett.* **2011**, *98*, 192901.

(18) Zhao, L.; Lu, Z.; Zhang, F.; Tian, G.; Song, X.; Li, Z.; Huang, K.; Zhang, Z.; Qin, M.; Wu, S.; Lu, X.; Zeng, M.; Gao, X.; Dai, J.; Liu, J. M. Current Rectifying and Resistive Switching in High Density $BiFeO_3$ Nanocapacitor Arrays on Nb-$SrTiO_3$ Substrates. *Sci. Rep.* **2015**, *5*, 9680.

(19) Chen, Y. N.; Wang, Z. J.; Yang, T.; Zhang, Z. D. Crystallization Kinetics of Amorphous Lead Zirconate Titanate Thin Films in a Microwave Magnetic Field. *Acta Mater.* **2014**, *71*, 1−10.

(20) Wang, Z.; Chen, Y.; Otsuka, Y.; Zhu, M.; Cao, Z.; Kokawa, H. Crystallization of Ferroelectric Lead Zirconate Titanate Thin Films by Microwave Annealing at Low Temperatures. *J. Am. Ceram. Soc.* **2011**, *94*, 404−409.

(21) Stemmer, S.; Streiffer, S. K.; Ernst, F.; Ruhle, M. Dislocations in $PbTiO_3$ Thin-Films. *Phys. Status Solidi A* **1995**, *147*, 135−154.

(22) Pintilie, I.; Teodorescu, C. M.; Ghica, C.; Chirila, C.; Boni, A. G.; Hrib, L.; Pasuk, I.; Negrea, R.; Apostol, N.; Pintilie, L. Polarization-Control of the Potential Barrier at the Electrode Interfaces in Epitaxial Ferroelectric Thin Films. *ACS Appl. Mater. Interfaces* **2014**, *6*, 2929−2939.

(23) Lee, D.; Jeon, B. C.; Yoon, A.; Shin, Y. J.; Lee, M. H.; Song, T. K.; Bu, S. D.; Kim, M.; Chung, J. S.; Yoon, J. G.; Noh, T. W. Flexoelectric Control of Defect Formation in Ferroelectric Epitaxial Thin Films. *Adv. Mater.* **2014**, *26*, 5005−11.

(24) Jeon, B. C.; Lee, D.; Lee, M. H.; Yang, S. M.; Chae, S. C.; Song, T. K.; Bu, S. D.; Chung, J. S.; Yoon, J. G.; Noh, T. W. Flexoelectric Effect in the Reversal of Self-Polarization and Associated Changes in the Electronic Functional Properties of $BiFeO_3$ Thin Films. *Adv. Mater.* **2013**, *25*, 5643−9.

(25) Han, M. G.; Marshall, M. S.; Wu, L.; Schofield, M. A.; Aoki, T.; Twesten, R.; Hoffman, J.; Walker, F. J.; Ahn, C. H.; Zhu, Y. Interface-Induced Nonswitchable Domains in Ferroelectric Thin Films. *Nat. Commun.* **2014**, *5*, 4693.

(26) Yuan, G. L.; Yang, Y.; Or, S. W. Aging-Induced Double Ferroelectric Hysteresis Loops in $BiFeO_3$ Multiferroic Ceramic. *Appl. Phys. Lett.* **2007**, *91*, 122907.

(27) Hu, W.; Wang, Z.; Du, Y.; Zhang, X. X.; Wu, T. Space-Charge-Mediated Anomalous Ferroelectric Switching in P(VDF-TrFE) Polymer Films. *ACS Appl. Mater. Interfaces* **2014**, *6*, 19057−19063.

(28) Lin, D.; Kwok, K. W.; Chan, H. L. W. Double Hysteresis Loop in Cu-Doped $K_{0.5}Na_{0.5}NbO_3$ Lead-Free Piezoelectric Ceramics. *Appl. Phys. Lett.* **2007**, *90*, 232903.

(29) Maksymovych, P.; Jesse, S.; Yu, P.; Ramesh, R.; Baddorf, A. P.; Kalinin, S. V. Polarization Control of Electron Tunneling into Ferroelectric Surfaces. *Science* **2009**, *324*, 1421−1425.

(30) Hong, S.; Choi, T.; Jeon, J. H.; Kim, Y.; Lee, H.; Joo, H. Y.; Hwang, I.; Kim, J. S.; Kang, S. O.; Kalinin, S. V.; Park, B. H. Large Resistive Switching in Ferroelectric $BiFeO_3$ Nano-Island Based Switchable Diodes. *Adv. Mater.* **2013**, *25*, 2339−2343.

(31) Lu, H.; Bark, C. W.; Esque de los Ojos, D.; Alcala, J.; Eom, C. B.; Catalan, G.; Gruverman, A. Mechanical Writing of Ferroelectric Polarization. *Science* **2012**, *336*, 59−61.

(32) Kim, T. H.; Jeon, B. C.; Min, T.; Yang, S. M.; Lee, D.; Kim, Y. S.; Baek, S.-H.; Saenrang, W.; Eom, C.-B.; Song, T. K.; Yoon, J.-G.; Noh, T. W. Continuous Control of Charge Transport in Bi-Deficient $BiFeO_3$ films through Local Ferroelectric Switching. *Adv. Funct. Mater.* **2012**, *22*, 4962−4968.

(33) Pintilie, L.; Vrejoiu, I.; Hesse, D.; LeRhun, G.; Alexe, M. Ferroelectric Polarization-Leakage Current Relation in High Quality Epitaxial $Pb(Zr,Ti)O_3$ Films. *Phys. Rev. B: Condens. Matter Mater. Phys.* **2007**, *75*, 104103.

(34) Pintilie, L.; Stancu, V.; Trupina, L.; Pintilie, I. Ferroelectric Schottky Diode Behavior from a $SrRuO_3$-$Pb(Zr_{0.2}Ti_{0.8})O_3$-Ta Structure. *Phys. Rev. B: Condens. Matter Mater. Phys.* **2010**, *82*, 085319.

(35) Das, R. R.; Bhattacharya, P.; Katiyar, R. S.; Bhalla, A. S. Leakage Current Behavior of $SrBi_2Ta_2O_9$ Ferroelectric Thin Films on Different Bottom Electrodes. *J. Appl. Phys.* **2002**, *92*, 6160.

(36) Boerasu, I.; Pintilie, L.; Pereira, M.; Vasilevskiy, M. I.; Gomes, M. J. M. Competition between Ferroelectric and Semiconductor Properties in $Pb(Zr_{0.65}Ti_{0.35})O_3$ Thin Films Deposited by Sol−Gel. *J. Appl. Phys.* **2003**, *93*, 4776.

(37) Setter, N.; Damjanovic, D.; Eng, L.; Fox, G.; Gevorgian, S.; Hong, S.; Kingon, A.; Kohlstedt, H.; Park, N. Y.; Stephenson, G. B.; Stolitchnov, I.; Taganstev, A. K.; Taylor, D. V.; Yamada, T.; Streiffer, S. Ferroelectric Thin Films: Review of Materials, Properties, and Applications. *J. Appl. Phys.* **2006**, *100*, 051606.

(38) Lee, D.; Baek, S. H.; Kim, T. H.; Yoon, J.-G.; Folkman, C. M.; Eom, C. B.; Noh, T. W. Polarity Control of Carrier Injection at Ferroelectric/Metal Interfaces for Electrically Switchable Diode and Photovoltaic Effects. *Phys. Rev. B: Condens. Matter Mater. Phys.* **2011**, *84*, 125305.

(39) Pintilie, L.; Alexe, M. Metal-Ferroelectric-Metal Heterostructures with Schottky Contacts. I. Influence of the Ferroelectric Properties. *J. Appl. Phys.* **2005**, *98*, 124103.

(40) Pintilie, L.; Boerasu, I.; Gomes, M. J. M.; Zhao, T.; Ramesh, R.; Alexe, M. Metal-Ferroelectric-Metal Structures with Schottky Contacts. Ii. Analysis of the Experimental Current-Voltage and Capacitance-Voltage Characteristics of $Pb(Zr,Ti)O_3$ Thin Films. *J. Appl. Phys.* **2005**, *98*, 124104.

(41) Khassaf, H.; Ibanescu, G. A.; Pintilie, I.; Misirlioglu, I. B.; Pintilie, L. Potential Barrier Increase Due to Gd Doping of $BiFeO_3$ Layers in Nb:$SrTiO_3$-$BiFeO_3$-Pt Structures Displaying Diode-Like Behavior. *Appl. Phys. Lett.* **2012**, *100*, 252903.

(42) Zhang, W.; Gao, Y.; Kang, L.; Yuan, M.; Yang, Q.; Cheng, H.; Pan, W.; Ouyang, J. Space-Charge Dominated Epitaxial $BaTiO_3$ Heterostructures. *Acta Mater.* **2015**, *85*, 207−215.

(43) Yang, H.; Luo, H. M.; Wang, H.; Usov, I. O.; Suvorova, N. A.; Jain, M.; Feldmann, D. M.; Dowden, P. C.; DePaula, R. F.; Jia, Q. X. Rectifying Current-Voltage Characteristics of $BiFeO_3$/Nb-Doped $SrTiO_3$ Heterojunction. *Appl. Phys. Lett.* **2008**, *92*, 102113.

(44) Robertson, J. Band Offsets of Wide-Band-Gap Oxides and Implications for Future Electronic Devices. *J. Vac. Sci. Technol., B: Microelectron. Process. Phenom.* **2000**, *18*, 1785−1791.

DOI: 10.1021/acsami.6b10992
ACS Appl. Mater. Interfaces 2016, 8, 32948−32955